Pergamon

Int. J. Heat Mass Transfer. Vol. 38, No. 1, pp. 65–70, 1995

0017-9310/95 $9.50+0.00

0017-9310(94)00152-9

Planar solidification of a finite slab: effects of the pressure dependence of the freezing point

M. CONTI

Dipartimento di Matematica e Fisica, Universita' di Camerino, 62032 Camerino, Italy

(*Received* 13 *January* 1994 *and in final form* 25 *April* 1994)

Abstract—Planar solidification in a slab of finite thickness is numerically simulated. The solid density is assumed to be lower than the liquid density and the phase change material expands while freezing (e.g. water). The effects of an opposing elastic force, due to the interaction with the container, are analysed. The increasing pressure determines a continuous lowering of the melting temperature; as a result the interface motion and the temperature field are strongly affected. The time square-root dependence of the melting front position fails down and is replaced by an asymptotic behaviour.

1. INTRODUCTION

The solution of Stefan problems describing solidification or melting of a phase change material (PCM) attracted considerable interest, due to the difficulties associated with the intrinsic non-linearity of the interface conditions and the unknown location of the melting front. Exact solutions are limited in number. Those found up to 1990 are discussed in ref. [1]. Several approximate methods have been developed and widely used, including quasi-steady methods, the heat balance integral concept [2], and variational methods [3]. Numerical solutions have been obtained, based on both fixed [4, 5] and variable [6, 7] grid methods.

Few solutions take into account the mechanical effects inherent in the phase change processes. Such effects may be due to the different density of the solid and the liquid phases: the PCM contracts or expands during the change of phase and convective terms arise in the heat equation. Analytical [8, 9] and numerical [10, 11] studies on this subject are mainly concerned with the kinematic effects of the volume change. However, melting or freezing of a PCM often takes place in a limited volume, bounded by the container walls. In this case, when the emerging phase is the one with lower density, the pressure exerted on the PCM increases and the melting temperature is affected according to the Clapeyron equation; the change of phase continues until either the breakdown of the container walls occurs, or the PCM reaches thermal equilibrium with the environment. No attempts have been made to address such a problem, that is of central relevance in geological processes as well as in many areas of engineering applications. Sliding of glaciers, for instance, is mainly driven by melting under high pressure conditions [12]. In soil physics, mechanical restrictions on the freezing of water are often encountered; as a result, ice can rarely form inside a soil mass at 0°C [13]. In the engineering of thermal storage severe mechanical conditions can arise when the melting PCM is surrounded by the solid phase, and hence is hindered to expand [14].

In the present paper, the one-dimensional solidification of a finite slab is numerically analysed. The PCM is assumed to expand while freezing. As shown in Fig. 1 the process is contrasted by a force that simulates, according to Hooke's law, the elastic behaviour of the container wall. Due to the increasing pressure a continuous lowering of the melting temperature occurs; the heat flux is reduced and the melting front advancement is slowed down.

The convective term in the heat equation, due to the expansion of the PCM, leads to a correction in the interface motion given by the product of the relative density change and the Stefan number [15]. Usually, both these parameters are rather small and the correction is quite small too. Hence, the pure diffusion equation has been utilised to treat the heat transfer inside the PCM. No pressure dependence of the PCM latent heat is assumed; equal values of the effective compressibility are assumed for the two phases.

The problem has been formulated through the weak solution approach usually referred to as the enthalpy method; the resulting equation has been solved numerically by the finite difference method.

The results that will be presented show that the interface motion is strongly affected by the pressure increase; the time square-root dependence of the melting front position fails down, and is replaced by an asymptotic behaviour.

2. FORMULATION OF THE PROBLEM

The system is illustrated in Fig. 1, where the emerging solid phase is represented by the shaded area and a spring simulates the elastic behaviour of the opposing container wall. Figure 2 shows, in a pressure–volume diagram, the thermodynamic path followed by the

NOMENCLATURE

a	thermal diffusivity
c	specific heat capacity
E	Young modulus of the elastic opposing wall
F	non-dimensional parameter, defined as: $F = (1/\lambda)(1/\rho_s - 1/\rho_l)(1-\rho_s/\rho_l)E/(\eta E+1)$
G	non-dimensional parameter, defined as: $G = T_{m0}/(T_{m0}-T_s)$
k	thermal conductivity
L	length of the PCM slab
L_0	initial length of the PCM slab
p	pressure
p_0	initial pressure of the PCM
St	Stefan number, defined as: $St = c_s(T_{m0}-T_s)/\lambda$
T	temperature
T_0	initial temperature of the PCM
T_m	actual melting temperature of the PCM
T_{m0}	initial melting temperature of the PCM
T_s	PCM temperature at $x = 0$
$\hat{T}$	dimensionless temperature, defined as: $\hat{T} = (T-T_{m0})/(T_{m0}-T_s)$
t	time
U	internal energy per unit volume
$\hat{U}$	dimensionless internal energy, defined as: $\hat{U} = (U-\rho_s c_s T_{m0})/(\rho_l \lambda)$
V	volume of the PCM
V_0	initial volume of the PCM
x	coordinate direction
x_f	coordinate of the melting front.

Greek symbols

η	effective compressibility of the PCM
λ	PCM latent heat
ξ	dimensionless coordinate direction, defined as: $\xi = x/L_0$
ξ_f	dimensionless coordinate of the melting front
ρ	density
σ	liquid fraction of the PCM
τ	dimensionless time, defined as: $\tau = a_s t/L_0^2$
χ	non-dimensional variable, defined as: $\chi = k_p/k_s$.

Subscripts

f	melting front
l	liquid phase of the PCM
p	PCM
s	solid phase of the PCM
0	initial conditions.

PCM; curves of constant liquid fraction of the PCM are labeled as σ_1, σ_2, σ_3. Let L_0, V_0 be the initial length and volume of the PCM slab. For times $t \leqslant 0$ the PCM is in the liquid phase at a uniform temperature $T(x, 0) = T_0 > T_{m0}$, where T_{m0} is the melting temperature at the initial pressure p_0. At time $t = 0$ the temperature of the surface $x = 0$ is suddenly lowered and maintained at $T(0, t) = T_s < T_{m0}$. Adiabatic wall at $x = L_0$ is assumed. A solid layer grows adjacent to the surface $x = 0$ and advances with time. The volume increase of the PCM, due to the lower density of the solid phase, is allowed in the x direction only, i.e. perfectly rigid lateral walls are assumed. The opposing wall causes a pressure increase on the PCM given, in the elastic limit, by:

$$p - p_0 = E\frac{(V-V_0)}{V_0}, \tag{1}$$

where p, V indicate the actual pressure and volume of

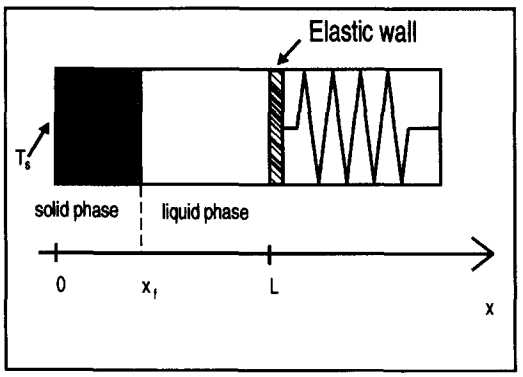

Fig. 1. Schematic diagram of the slab and the opposing elastic wall. The shaded area represents the emerging solid phase; the spring simulates the elastic behaviour of the opposing wall at $x = L$.

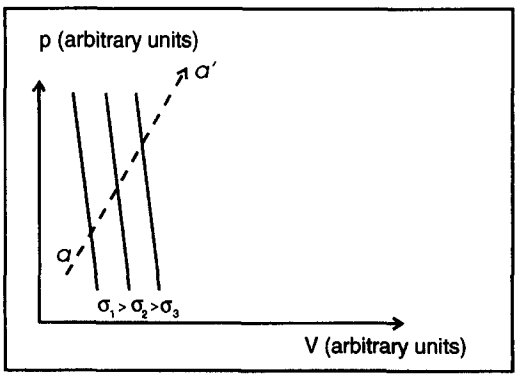

Fig. 2. The thermodynamic path along the straight line aa' followed by the PCM in the pressure–volume plane. Curves of constant PCM liquid fraction are labeled as $\sigma_1, \sigma_2, \sigma_3$.

the PCM and E is the Young's modulus of the elastic wall. Equation (1) is represented, in Fig. 2, by the straight line aa'. The PCM volume is determined by solving equation (1) in conjunction with:

$$p-p_0 = -\frac{1}{\eta}\frac{(V-V')}{V'}. \tag{2}$$

Equation (2) describes the compression of the PCM and is represented by the curves labelled as σ; η is the effective compressibility of the two-phase mixture; and V' is the volume that would be occupied by the PCM in absence of opposing forces. It is easy to show that:

$$V' = V_0\left[1+\left(1-\frac{\rho_s}{\rho_l}\right)\frac{x_f}{L_0}\right]. \tag{3}$$

When $(1-(\rho_s/\rho_l))$ is small, as is usually the case, equations (2) and (3) give:

$$p-p_0 = \frac{E}{\eta E+1}\left(1-\frac{\rho_s}{\rho_l}\right)\frac{x_f}{L_0}. \tag{4}$$

Equation (4) shows that the pressure of the system increases as the solidification goes on; as a consequence the melting temperature changes according to the Clapeyron equation:

$$\frac{dp}{dT_m} = \frac{\lambda}{T_m(\rho_l^{-1}-\rho_s^{-1})}. \tag{5}$$

If the PCM latent heat is not affected by the pressure variation, equation (5) can be easily integrated to give:

$$T_m = T_{m0}\cdot\exp -\frac{(\rho_s^{-1}-\rho_l^{-1})}{\lambda}(p-p_0). \tag{6}$$

In the following it will be assumed that:

- the heat transfer is only due to conduction, i.e. the kinematic effects of the phase change are neglected;
- the energy interaction due to mechanical work is neglected too.

It means that density variations during the process are ignored except insofar as they give rise to a pressure increase.

Under these assumptions, the one-dimensional heat equation can be written as

$$\frac{\partial U}{\partial t} = \frac{\partial}{\partial x}k_p\frac{\partial T}{\partial x}. \tag{7}$$

U in equation (7) indicates the energy stored per unit volume, and is related to the temperature via:

$$T = \alpha U+\beta, \tag{8}$$

where:

$$\alpha = (\rho_s c_s)^{-1} \quad \beta = 0 \quad \{U \leqslant \rho_s c_s T_m\},$$

$$\alpha = 0 \quad \beta = T_m \quad \left\{0 \leqslant \frac{U-\rho_s c_s T_m}{\rho_l \lambda} \leqslant 1\right\},$$

$$\alpha = (\rho_l c_l)^{-1} \quad \beta = T_m\left(1-\frac{\rho_s c_s}{\rho_l c_l}\right)-\frac{\lambda}{c_l}$$

$$\left\{\frac{U-\rho_s c_s T_m}{\rho_l \lambda} > 1\right\}.$$

The initial and boundary conditions for equation (7) are specified by:

$$T(x,0) = T_0 \quad T(0,t) = T_s \quad \left.\frac{\partial T}{\partial x}\right|_{x=L_0} = 0.$$

The problem can be conveniently restated in terms of the following non-dimensional variables:

$$\xi = x/L_0 \quad \tau = a_s t/L_0^2 \quad \hat{T} = (T-T_{m0})/(T_{m0}-T_s)$$

$$\chi = k_p/k_s \quad St = c_s(T_{m0}-T_s)/\lambda$$

$$\hat{U} = (U-\rho_s c_s T_{m0})/(\rho_l \lambda)$$

$$F = \left(\frac{1}{\rho_s}-\frac{1}{\rho_l}\right)\left(1-\frac{\rho_s}{\rho_l}\right)\frac{E}{\eta E+1}\frac{1}{\lambda} \quad G = \frac{T_{m0}}{T_{m0}-T_s}.$$

The non-dimensional melting temperature is given by:

$$\hat{T}_m = G(e^{-F\xi_f}-1). \tag{9}$$

The dimensionless energy equation can be written as follows:

$$\frac{1}{St}\frac{\rho_l}{\rho_s}\frac{\partial \hat{U}}{\partial \tau} = \frac{\partial}{\partial \xi}\chi\frac{\partial \hat{T}}{\partial \xi}, \tag{10}$$

with the initial and boundary conditions specified as follows:

$$\hat{T}(\xi,0) = \hat{T}_0 \quad \hat{T}(0,\tau) = -1 \quad \left.\frac{\partial \hat{T}}{\partial \xi}\right|_{\xi=1} = 0.$$

The non-dimensional energy is related to the temperature via:

$$\hat{T} = \hat{\alpha}\hat{U}+\hat{\beta} \tag{11}$$

where:

$$\hat{\alpha} = \frac{\rho_l}{\rho_s}\frac{1}{St} \quad \hat{\beta} = 0 \quad \left\{\hat{U} \leqslant \hat{T}_m St\cdot\frac{\rho_s}{\rho_l}\right\}$$

$$\hat{\alpha} = 0 \quad \hat{\beta} = \hat{T}_m \quad \left\{\hat{T}_m St\frac{\rho_s}{\rho_l} \leqslant \hat{U} \leqslant 1+\hat{T}_m St\frac{\rho_s}{\rho_l}\right\}$$

$$\hat{\alpha} = \frac{c_s}{c_l}\frac{1}{St} \quad \hat{\beta} = \hat{T}_m\left(1-\frac{\rho_s c_s}{\rho_l c_l}\right)-\frac{c_s}{c_l}\frac{1}{St}$$

$$\left\{\hat{U} \geqslant 1+\hat{T}_m St\frac{\rho_s}{\rho_l}\right\}.$$

It can be observed that the temperature field inside the PCM depends on $\xi, \tau, St, F, G, \rho_l/\rho_s, \chi, c_l/c_s, \hat{T}_0$.

3. THE NUMERICAL PROCEDURE

The energy equation has been approximated with the control-volume finite-difference approach suggested by Patankar [16]. The resulting algebraic equa-

tions have been solved by the tridiagonal matrix algorithm.

The solid–liquid interface, needed to determine the actual melting temperature through equation (9), is identified at the discontinuity of the energy per unit volume field. During the process the PCM melting temperature is updated by using the following procedure: at each time step the problem is solved with the 'old' melting temperature, then the freezing front is identified. The new melting temperature is evaluated and the problem is solved again. The procedure is repeated until convergence is attained. The converged results are assumed to be reached when the maximum relative change of the variables between consecutive iterations is less than 0.01%. This is a simple way to track with a trial and error technique the actual thermodynamic path followed by the PCM.

The consistency of the computational scheme has been checked by performing an overall energy balance at each time step: energy conservation was verified within 0.01% of the total heat removed from the PCM. However, the enthalpy method applied to phase change problems can result in unaccurate temperature history and distribution inside the PCM, and careful attention must be paid in choosing the grid spacing as well as the time step. The check on the energy conservation is not effective to stress these difficulties, because it is basically tautologic in respect to the primitive equation. The entropy equation provides an alternative and independent way to verify the accuracy of the temperature field [17]. The entropy balance has been performed at each time step; the numerical source of entropy never exceeded 0.5% of the entropy generated inside the PCM.

4. RESULTS

The lack of experimental data makes it difficult to validate the present model. However, for low values of the Stefan number, the numerical solution can be tested against a quasi-steady approximation. When linear temperature profiles are assumed in the solid and liquid phases, and as long as the PCM temperature at $x = L_0$ is tied to T_0, the heat balance at the interface is:

$$\frac{dx_f}{dt} = \frac{1}{\rho_s \lambda}\left\{\frac{k_s}{x_f}[T_m(x_f) - T_s] - \frac{k_l}{L_0 - x_f}[T_0 - T_m(x_f)]\right\}, \tag{12}$$

where the actual melting temperature is related to the melting front position through equation (6).

In terms of the non-dimensional variables, and when F is small, the heat balance becomes, after some manipulations:

$$d\tau = \frac{\xi_f(1-\xi_f)}{St\,FG(1-k_l/k_s)\xi^2 - St(1+FG+\hat{T}_0 k_l/k_s)\xi_f + St}\,d\xi_f. \tag{13}$$

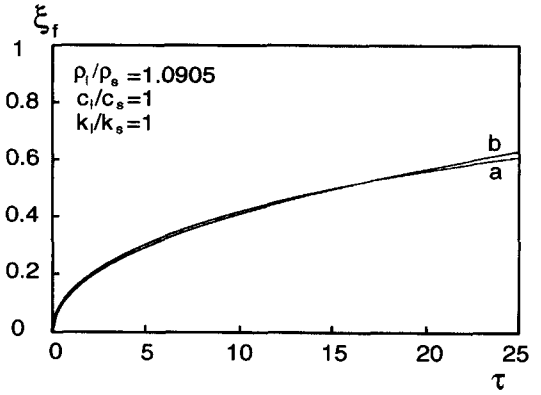

Fig. 3. The melting front position vs the non-dimensional time. Curve a represents the quasi-steady solution, curve b the present numerical solution. $St = 0.01$; $F = 0.003$; $G = 101$; $\hat{T}_0 = 0$.

Equation (13) can easily be integrated to give the advancement of the melting front; when $k_l/k_s = 1$ the solution is:

$$\tau = \frac{\xi_f}{B} - \left(\frac{St^2}{B^3} + \frac{St}{B^2}\right)\ln\left(\frac{B\xi_f}{St} + 1\right) - \frac{\xi_f}{2B^2}(B\xi - 2St), \tag{14}$$

with $B = -St(1 + FG + \hat{T}_0)$.

Figure 3 shows the melting front position vs τ, with $F = 3 \times 10^{-3}$, $St = 10^{-2}$; curve a refers to the quasi-steady solution and curve b to the numerical solution. It can be observed that the agreement is quite satisfactory at low τ values; when τ becomes large the PCM temperature at $x = L_0$ is driven towards T_s and the quasi-steady model fails down.

On the side of large τ values, the asymptotic melting front position can be derived through equation (9): it results, when thermal equilibrium is attained, in:

$$\xi_f = \frac{1}{F}\ln\frac{G}{G-1}. \tag{15}$$

Figure 4 shows the asymptotic melting front position

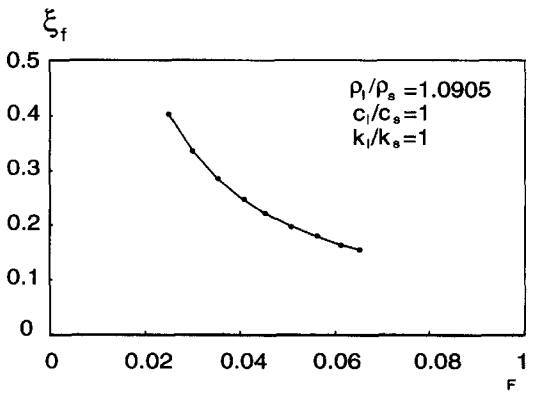

Fig. 4. The asymptotic melting front position vs F: the solid curve is drawn through equation (15), the dots refer to the numerical solution. $St = 0.01$; $G = 101$; $\hat{T}_0 = 0$.

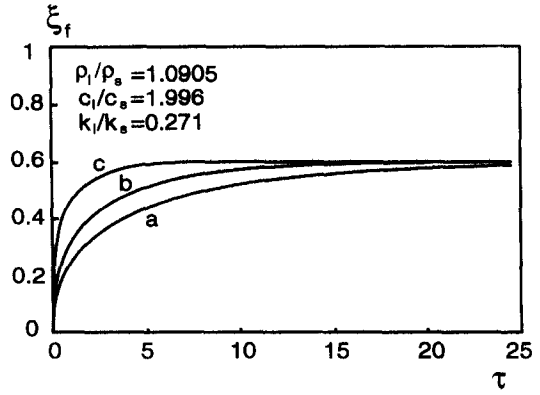

Fig. 5. The melting front position vs the non-dimensional time for different values of the Stefan number. $F = 0.1$; $G = 17.7$; $\hat{T}_0 = 0$. Curve a: $St = 0.05$; curve b: $St = 0.1$; curve c: $St = 0.5$.

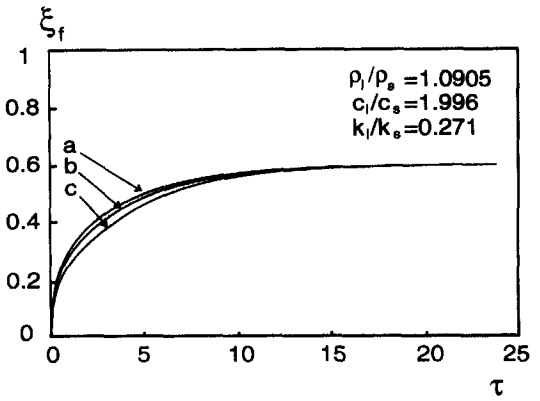

Fig. 8. The melting front position vs the non-dimensional time for different values of the initial PCM temperature. $St = 0.1$; $F = 0.1$; $G = 17.7$. Curve a: $\hat{T}_0 = 0$; curve b: $\hat{T}_0 = 1$; curve c: $\hat{T}_0 = 2$.

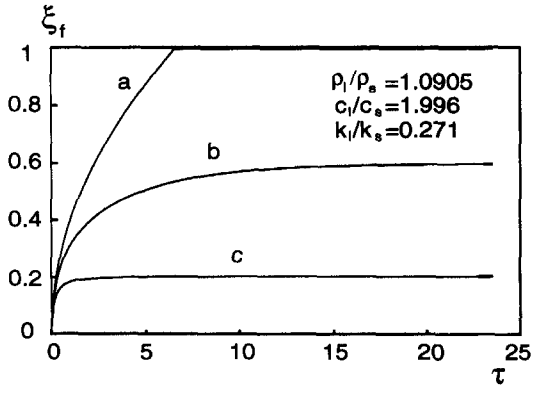

Fig. 6. The melting front position vs the non-dimensional time for different values of F. $St = 0.1$; $G = 17.7$; $\hat{T}_0 = 0$. Curve a: $F = 0.01$; curve b: $F = 0.1$; curve c: $F = 0.3$.

vs F: the solid curve is drawn through equation (15), the dots refer to the numerical solution. As it can be observed, the agreement is excellent.

Now we are going to see how the melting front advancement is affected by variations of $St, F, G, \hat{T}_0$. The remaining non-dimensional parameters have been chosen with reference to the thermophysical properties of water.

The effect of the Stefan number is represented in Fig. 5. Here $\hat{T}_0 = 0$, $F = 0.1$ and $G = 17.17$. The melting front saturates at $\xi_f = 0.6$. The curves show how faster thermal equilibrium is attained as the Stefan number increases.

Figure 6 shows the influence of F, i.e. of the mechanical constriction on the PCM. At $F = 0.01$ thermal equilibrium is attained when all the PCM is solidified. As F increases the velocity of the melting front is reduced and the liquid fraction of the PCM at thermal equilibrium increases, as indicated by equation (15).

A similar role is played by G, as shown in Fig. 7; equation (9) indeed indicates that for low F values F and G affect the solution merely through their product.

Figure 8 shows the effect of the initial overheating of the PCM. The curves indicate that as $\hat{T}_0$ increases the adverse temperature gradient reduces the melting front velocity, but does not affect the saturation value ξ_f.

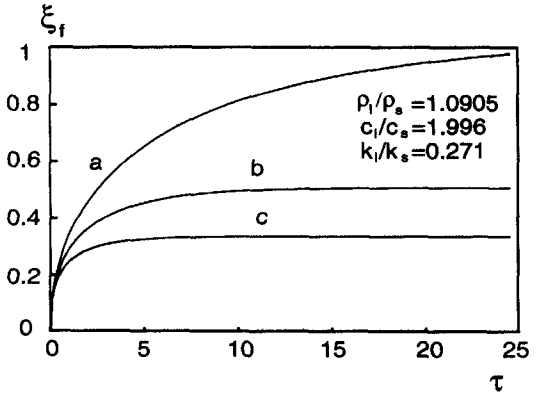

Fig. 7. The melting front position vs the non-dimensional time for different values of G. $St = 0.1$; $F = 0.1$; $\hat{T}_0 = 0$. Curve a: $G = 10$; curve b: $G = 20$; curve c: $G = 30$.

5. CONCLUSIONS

In this paper we analysed the planar solidification in a slab of finite thickness; attention has been focused on the effects of the pressure increase due to the density change in the phase transition. The problem is of great interest in geological processes as well as in many areas of engineering applications and, to the author's knowledge, has never been addressed in the literature.

The results show the influence of some parameters on the melting front advancement and on the thermal equilibrium end state.

REFERENCES

1. V. J. Lunardini, *Heat Transfer with Freezing and Thawing*. Elsevier, New York (1991).
2. T. R. Goodman, Heat balance integral: further con-

siderations and refinements, *J. Heat Transfer* **83,** 83–86 (1961).
3. M. A. Biot and H. Daughaday, Variational analysis of ablation, *J. Aerospace Sci.* **29,** 227–229 (1962).
4. V. Voller and M. Cross, Accurate solutions of moving boundary problems using the enthalpy method, *Int. J. Heat Mass Transfer* **24,** 545–556 (1981).
5. Y. Cao and A. Faghri, A temperature transforming model with a fixed grid numerical methodology for phase change problems including natural convection, *J. Heat Transfer* **112,** 812–816 (1990).
6. W. D. Murray and F. Landis, Numerical and machine solutions of transient heat conduction problems involving melting or freezing, *J. Heat Transfer* **81,** 106–112 (1959).
7. C. F. Hsu, E. M. Sparrow and S. V. Patankar, Numerical solution of moving boundary problems by boundary immobilization and a control-volume based finite-difference scheme, *Int. J. Heat Mass Transfer* **24,** 1335–1343 (1981).
8. E. R. G. Eckert and R. M. Drake, *Analysis of Heat and Mass Transfer*. McGraw-Hill, London (1972).
9. J. Crank, *The Mathematics of Diffusion*. Clarendon, Oxford (1956).
10. C.-J. Kim and M. Kaviany, A numerical method for phase-change problems, *Int. J. Heat Mass Transfer* **33,** 2721–2734 (1990).
11. C.-J. Kim and M. Kaviany, A numerical method for phase-change problems with convection and diffusion, *Int. J. Heat Mass Transfer* **35,** 457–467 (1992).
12. W. S. B. Paterson, *The Physics of Glaciers* (2nd Edn), p. 112. Pergamon Press, Oxford (1981).
13. D. Hillel, *Applications of Soil Physics*, p. 257. Academic Press, New York (1980).
14. S. Weingartner and J. Blumenberg, Experimental and theoretical analysis of heat of fusion storage for solar dynamic power systems. In *Forty-first Congress of the International Astronautical Federation*. Dresden, Germany (October 1990).
15. Ch. Charach and Y. Zarmi, Planar solidification in a finite slab: effects of density change, *J. Appl. Phys.* **70,** 6687–6693 (1991).
16. S. V. Patankar, *Numerical Heat Transfer and Fluid Flow*. Hemisphere, Washington, DC (1980).
17. C. Bellecci and M. Conti, Phase change energy storage: entropy production, irreversibility and second-law efficiency, *Solar Energy* (in press).